Inorganic Chemistry

1-D Polymers with Alternate Cu_2 and Ln_2 Units (Ln = Gd, Er, Y) and Carboxylate Linkages

Rafael Calvo,*,† Raul E. Rapp,‡ Edson Chagas,‡ Rosana P. Sartoris,† Ricardo Baggio,§ María T. Garland,‖ and Mireille Perec*,⊥

Facultad de Bioquímica y Ciencias Biológicas, Universidad Nacional del Litoral, and INTEC (CONICET-UNL), Güemes 3450, 3000 Santa Fe, Argentina, Universidade Federal do Rio de Janeiro, CP 68528, Rio de Janeiro 21941-972, RJ, Brazil, Comisión Nacional de Energía Atómica, Av. Gral. Paz 1499, 1650 San Martín, Buenos Aires, Argentina, Facultad de Ciencias Físicas y Matemáticas, Universidad de Chile, Av. Blanco Encalada 2008, Santiago, Chile, and INQUIMAE-DQIAQF, Facultad de Ciencias Exactas y Naturales, Universidad de Buenos Aires, Ciudad Universitaria, C1428EHA, Buenos Aires, Argentina

Three isostructural Cu_2Ln_2 1-D polymers $[Cu_2Ln_2L_{10}(H_2O)_4 \cdot 3H_2O]_n$ where Ln = Gd (**1**), Er (**2**), and Y (**3**) and HL= *trans*-2-butenoic acid, were synthesized and characterized by X-ray crystallography, electron paramagnetic resonance, and magnetic measurements. Pairs of alternate Cu_2 and Ln_2 dinuclear units are combined into a linear array by a set of one covalent $\eta^2:\eta^1:\mu_2$ carboxylate oxygen and two H bonds, at Cu···Ln distances of ca. 4.5 Å. These units exhibit four $\eta^1:\eta^1:\mu_2$ and two $\eta^2:\eta^1:\mu_2$ carboxylate bridges, respectively. Magnetic measurements between 2 and 300 K, fields $B_0 = \mu_0H$ between 0 and 9 T, and electron paramagnetic resonance (EPR) measurements at the X-band and room temperature are reported. The magnetic susceptibilities indicate bulk antiferromagnetic behavior of the three compounds at low temperatures. Magnetization and EPR data for **1** and **3** allowed evaluation of the exchange couplings between both Cu and Gd ions in their dinuclear units and between Cu and Gd neighbor ions in the spin chains. The data for the isolated Cu_2 units in **3** yield $g_{\parallel}$ = 2.350 and $g_\perp$ = 2.054, J_{Cu-Cu} = −338 (3) cm^{-1} for the exchange coupling $[H_{ex}(1,2) = -J_{1-2} \, S_1 \cdot S_2]$, and D_0 = −0.342 (0.003) cm^{-1} and E_0 = 0.003 (0.001) cm^{-1} for the zero-field-splitting parameters of the triplet state arising from anisotropic spin−spin interactions. Considering tetranuclear blocks Gd−Cu−Cu−Gd in **1**, with the parameters for the Cu_2 unit obtained for **3**, we evaluated ferromagnetic interactions between Cu and Gd neighbors, J_{Cu-Gd} = 13.0 (0.1) cm^{-1}, and between Gd ions in the Gd_2 units, J_{Gd-Gd} = 0.25 (0.02) cm^{-1}, with g_{Gd} = 1.991. The bulk antiferromagnetic behavior of **1** is a consequence of the antiferromagnetic coupling between Cu ions and of the magnitude, $|J_{Cu-Gd}|$, of the Cu−Gd exchange coupling. Compound **2** displays a susceptibility peak at 15 K that may be interpreted as the combined result from antiferromagnetic couplings between Er^{III} ions in Er_2 units and their coupling with the Cu_2 units.

Introduction

Hybrid inorganic−organic materials containing 3d and 4f cations connected by organic ligands are of interest because they combine the physical properties and reactivities of transition and lanthanide metal ions with the functionality of the organic linkers.[1−7] Multicarboxylic acids are extensively used in the construction of these materials, forming a large variety of interesting structures,[8] whereas aliphatic monocarboxylic acids have limited bonding options. Polymeric chainlike structures with monocarboxylate ligands have been reported for the isostructural trichloroacetates [Ln₂Cu

* Authors to whom correspondence should be addressed. E-mail: perec@qi.fcen.uba.ar (M.P.), calvo@fbcb.unl.edu.ar (R.C.).
† Universidad Nacional del Litoral and INTEC.
‡ Universidade Federal do Rio de Janeiro.
§ Comisión Nacional de Energía Atómica.
‖ Universidad de Chile.
⊥ Universidad de Buenos Aires.

(1) Cheetham, A. K.; Rao, C. N. R.; Feller, R. K. *Chem. Commun.* **2006**, *2006*, 4780−4795.
(2) Xu, Z. Q.; Read, P. W.; Hibbs, D. E.; Hursthouse, M. B.; Malik, K. M. A.; Patrick, B. O.; Rettig, S. J.; Seid, M.; Summers, D. A.; Pink, M.; Thompson, R. C.; Orvig, C. *Inorg. Chem.* **2000**, *39*, 508−516.

$(CCl_3COO)_8 \cdot 6H_2O]_n$ (Ln = Sm, Gd, and Nd).[9,10] Discrete pentanuclear $Cu^{II}-Ln^{III}$ chloroacetates $[Cu_3Ln_2(O_2CCH_2Cl)_{12}$ $(H_2O)_8] \cdot 2H_2O$ (Ln = Gd, Dy, Ho, Nd, and Yb)[11–14] are also known.

The magnetic and optical properties of molecular-based compounds having simultaneously 3d and 4f transition metal ions have attracted much attention because of their possible applications as molecular magnets[15–20] and luminescent materials.[21] Considering that the high magnetic moments and anisotropies of the lanthanides may be boosted by the larger interactions with the more expanded s, p, and d electrons, progress on the preparation and understanding of these materials is of increasing interest.[18] Single-chain magnets may also display slow magnetic relaxation, characteristic of single-molecule magnets.[22] Although many 3-D polymeric complexes of the type 3d–4f are known, it is interesting to obtain new 1-D 3d–4f compounds with alternation schemes of metal and lanthanide centers.

In the past few years, we and others have shown the potentiality of the monocarboxylate *trans*-2 butenoate ligand for the formation of homonuclear polymers of La^{III}, Pr^{III}, Nd^{III}, Eu^{III}, Gd^{III}, Tb^{III}, Dy^{III}, and Ho^{III}.[23–26] The reaction of *trans*-2-butenoic acid (HL) with $Cu(OH)_2$ in DMF led to dinuclear $Cu_2(L)_4(DMF)_2$, containing the classical paddle-wheel dimer[27] frequently used as a connection device in the self-assembly of magnetic materials.[28] We report here the synthesis, X-ray crystal structure, and magnetic properties of three isostructural 1-D arrays formulated as $[Cu_2Ln_2L_{10}$ $(H_2O)_4 \cdot 3H_2O]_n$ with Ln = Gd **1**, Er **2**, and Y **3** and HL= *trans*-2-butenoic acid, in which alternate dinuclear Cu_2 and Ln_2 units form 1-D chains parallel to the *a* crystal axis. These units are bridged by a covalent tridentate carboxylate oxygen and two H bonds. The three novel isostructural chains provide good model systems for magneto-structural correlations and other interaction studies. Compound **3** with diamagnetic Y^{III} allows study of the magnetic properties of the isolated Cu_2 dinuclear units and derivation of information for the isostructural compounds **1** and **2**.

Experimental Section

Materials. All reagents were commercially available chemicals of analytical- or reagent-grade purity and used as received. Water was purified by a Millipore milli-Q system, yielding 18 MΩ cm of water.

Synthesis of $[Cu_2Gd_2L_{10}(H_2O)_4 \cdot 3H_2O]_n$, 1. The dimeric compound $[Gd_2(L)_6(H_2O)_4] \cdot 2H_2O$ was first synthesized from Gd_2O_3 and *trans*-2-butenoic acid in water under hydrothermal conditions at 150 °C for 76 h and autogenous pressure, as described previously.[24] A mixture of $[Gd_2(L)_6(H_2O)_4] \cdot 2H_2O$ (0.90 g, 1 mmol) and copper acetate dihydrate (0.40 g, 2 mmol) was added into water (100 mL) under stirring, followed by the addition of *trans*-2-butenoic until the pH value of the system was adjusted to about 5. After being stirred for 10 h at 80 °C, the resulting solution was cooled to room temperature and passed through a glass filter. The filtrate was stored in a stoppered flask for two weeks, whereupon green crystals mixed with an amorphous dark material separated out. Recrystallization from methanol allowed the filtration of a material which was identified as Cu(*trans*-2-butenoate)$_2$ by elemental analysis and X-ray powder diffraction (see Figure S1 in the Supporting Information). Compound **1** was isolated from the filtrate as blue prismatic crystals in about 45% yield based on the copper salt. Anal. calcd for complex **1**, $C_{40}H_{64}O_{27}Cu_2Gd_2$: C, 33.85, H, 4.55, Cu, 9.00. Found: C, 34.60; H, 4.75; Cu, 9.10%.

Main FT-IR bands (KBr disk, cm^{-1}): 3427 (s, v br, ν(OH)), 1659, 1603 and 1538 (vs, ν(CO_2^-)asym), 1449 and 1417 (vs, ν(CO_2^-)sym), 1297(m), 1256(m), 1105(w), 967(m), 917(w), 857(w), 749(m), 699(w), 651(br, w), 521(w), 461(w), 420(w). Thermogravimetric analysis (TGA) showed that the first mass loss occurring in the range 80–112 °C corresponds to seven water molecules (three hydration and four coordination water molecules) per formula unit, calcd 8.8% and found 8.9%, suggesting that the water molecules are weakly bonded. Decomposition in the range 245–550 °C occurs in three overlapping steps. The final residual mass of ca. 64.3% suggests the formation of $CuGd_2O_4$ and CuO in a 1:1 ratio within 1.4%, as confirmed by X-ray diffraction (XRD).

Synthesis of $[Cu_2Er_2L_{10}(H_2O)_4 \cdot 3H_2O]_n$, 2, and $[Cu_2Y_2L_{10}(H_2O)_4 \cdot 3H_2O\}_n$, 3. A mixture of Ln_2O_3 (Ln = Er, Y; 1 mmol), *trans*-2-butenoic acid (0.90 g, 10 mmol), and copper(II) acetate monohydrate (0.40 g, 2 mmol) and water (100 mL) was heated to boiling under continuous stirring for 10 h and filtered while hot. The clear solution was allowed to cool at room temperature in a stoppered

(3) Wu, G.; Hewitt, I. J.; Mameri, S.; Lan, Y.; Clerac, R.; Anson, C. E.; Qiu, S.; Powell, A. K. *Inorg. Chem.* **2007**, *46*, 7229–7231.

(4) Osa, S.; Kido, T.; Matsumoto, N.; Re, N.; Pochaba, A.; Mrozinski, J. *J. Am. Chem. Soc.* **2004**, *126*, 420–421.

(5) Winpenny, R. E. P. *Chem. Soc. Rev.* **1998**, *27*, 447–452.

(6) Zhao, B.; Cheng, P.; Chen, X. Y.; Cheng, C.; Shi, W.; Liao, D. Z.; Yan, S. P.; Jiang, Z. H. *J. Am. Chem. Soc.* **2004**, *126*, 3012–3013.

(7) Gheorghe, R.; Cucos, P.; Andruh, M.; Costes, J. P.; Donnadieu, B.; Shova, S. *Chem.—Eur. J.* **2006**, *12*, 187–203.

(8) Rao, C. N. R.; Natarajan, S.; Vaihyanathan, R. *Angew. Chem., Int. Ed.* **2004**, *43*, 1466–1496.

(9) Kutlu, I.; Meyer, G.; Oczko, G.; Legendziewicz, J. *Eur. J. Sol. St. Inorg. Chem* **1997**, *34*, 231–238.

(10) Legendziewicz, J.; Borzechowska, M. G.; Oczko, G.; Meyer, G. *New J. Chem.* **2000**, *24*, 53–59.

(11) Chen, X.; Wu, Y.; Tong, Y.; Huang, X. *J. Chem. Soc., Dalton Trans.* **1996**, 2443–2448.

(12) Cui, Y.; Zheng, F. K.; Yan, D. C.; Chen, W. D.; Huang, J. S. *Jiegou Huaxue (Chinese J. Struct. Chem.)* **1998**, *17*, 5.

(13) Tong, M. L.; Wu, Y. L.; Chen, X. M.; Sun, Z. M.; Hendrickson, D. N. *Chem. Res. Chinese U.* **1998**, *14*, 230–235.

(14) Voronkova, V. K.; Galeev, R. T.; Shova, S.; Novitchi, G.; Turta, C. I.; Caneschi, A.; Gatteschi, D.; Lipkowski, J.; Simonov, Y. A. *Appl. Magn. Reson.* **2003**, *25*, 227–247.

(15) Kahn, O. *Molecular Magnetism*; VCH Publishers: New York, 1993.

(16) Bencini, A.; Benelli, C.; Caneschi, A.; Carlin, R. L.; Dei, A.; Gatteschi, D. *J. Am. Chem. Soc.* **1985**, *107*, 8128–8136.

(17) Bencini, A.; Benelli, C.; Caneschi, A.; Dei, A.; Gatteschi, D. *Inorg. Chem.* **1986**, *25*, 572–575.

(18) Benelli, C.; Gatteschi, D. *Chem. Rev.* **2002**, *102*, 2369–2387.

(19) Janiak, C. *Dalton Trans.* **2003**, *2003*, 2781–2804.

(20) Champness, N. R. *Dalton Trans.* **2006**, *2006*, 877–880.

(21) Reineke, T. M.; Eddaoudi, M.; Fehr, M.; Kelley, D.; Yaghi, O. M. *J. Am. Chem. Soc.* **1999**, *121*, 1651–1657.

(22) Coulon, C.; Miyasaka, H.; Clerac, R. *Struct. Bonding (Berlin)* **2006**, *122*, 163–206.

(23) Barja, B.; Baggio, R.; Garland, M. T.; Aramendia, P. F.; Peña, O.; Perec, M. *Inorg. Chim. Acta* **2003**, *346*, 187–196.

(24) Rizzi, A.; Baggio, R.; Garland, M. T.; Peña, O.; Perec, M. *Inorg. Chim. Acta* **2003**, *353*, 315–319.

(25) Atria, A. M.; Baggio, R.; Garland, M. T.; Muñoz, J. C.; Peña, O. *Inorg. Chim. Acta* **2004**, *357*, 1997–2006.

(26) Baggio, R.; Calvo, R.; Garland, M. T.; Peña, O.; Perec, M.; Rizzi, A. *Inorg. Chem.* **2005**, *44*, 8979–8987.

(27) Schlam, R. F.; Perec, M.; Calvo, R.; Lezama, L.; Insausti, M.; Rojo, T.; Foxman, B. M. *Inorg. Chim. Acta* **2000**, *310*, 81–88.

(28) Rowsell, J. L. C.; Spencer, E. C.; Eckert, J.; Howard, J. A. K.; Yaghi, O. M. *Science* **2005**, *309*, 1350–1354.

flask. After one month, thin green-blue needles of **2** and **3** suitable for X-ray crystallographic work separated out and were carefully collected and dried in the air (the yield in both cases was around 75% based on Ln_2O_3). Optical examination, combined with X-ray powder diffraction, indicated phase purity in both cases and that they were isostructural. Anal. calcd for complex **2**, $C_{40}H_{64}O_{27}$-Cu_2Er_2: C, 33.40; H, 4.48; Cu, 8.85. Found: C, 33.70; H, 4.50; Cu, 8.80%. Anal. calcd for complex **3**, $C_{40}H_{64}O_{27}Cu_2Y_2$: C, 37.50; H, 5.05; Cu, 9.92. Found: C, 37.60; H, 5.10; Cu, 10.00%. The IR spectra for compounds **2** and **3** are similar to that of complex **1**, with absorption bands within ± 10 cm^{-1}. The TGA profiles for **2** and **3** are almost identical to that of **1**.

Physical Measurements. Elemental analyses of C and H were performed on a Carlo Erba 1108 elemental analyzer. Copper content was determined on a Shimadzu AA6501 spectrophotometer. Infrared spectra were recorded as KBr pellets and as Nujol mulls on a Nicolet 510P FT-IR spectrophotometer. Thermogravimetric measurements were carried out using a Shimadzu DTG 50 thermal analyzer under an air flow of 40 L/min at a heating rate of 5 °C min^{-1}. The purity of the products was checked by X-ray powder diffraction using monochromated Cu Kα radiation on a Phillips X'Pert diffractometer.

Electron paramagnetic resonance (EPR) spectra of powdered samples of **1**, **2**, and **3** were collected at 300 K with a Bruker ER-200 spectrometer working at 9.7 GHz using a 12-in. magnet and a cavity with 100 kHz field modulation. The spectra were analyzed using EasySpin,[29,30] an EPR simulation package working under Matlab.[31] Some features of this package were also used to evaluate magnetic properties.

Magnetic measurements were performed with a commercial PPMS magnetometer with the ACMS option (Quantum Design, Inc., San Diego, CA) in powder samples of about 40 mg using cylindrical sample holders of 2 mm i.d. and 12 mm height. The contribution of the sample holders was measured at the same temperatures and magnetic field and subtracted from the data. In the cases of **1** and **2**, this contribution is less than 2% of the sample contribution, but it is more important for **3**. In all measurements, the field was taken to zero at 300 K; the samples were cooled, and the field was applied at ~2 K (zero-field cooling).

X-Ray Crystallography. Data for $[Cu_2Ln_2L_{10}(H_2O)_4 \cdot 3H_2O]_n$ where Ln = Gd (**1**), Er (**2**), and Y (**3**) were collected on a Bruker AXS SMART APEX CCD diffractometer using monochromatic Mo Kα radiation ($\lambda = 0.71069$Å). As the driving software and data integration, we used the programs *SMART*[32] and *SAINT*.[33] Semiempirical absorption corrections were applied using *SADABS*.[34] The structure was solved by direct methods and difference Fourier and refined by least-squares on F^2 with anisotropic displacement parameters for non-H atoms. Hydrogen atoms defined by the stereochemistry were placed at their calculated positions and allowed to ride onto their host carbons both in coordinates as well as in thermal parameters. Those corresponding to water molecules were not found in the final difference Fourier maps and were accordingly disregarded in the model. All calculations to solve the structures, refine the models, and obtain derived results were carried out with the computer programs SHELXS97, SHELXL97,[35] and SHELXTL.[36] Full use of the CCDC package was also made for searching in the CSD Database.[37]

Crystallographic data (excluding structure factors) for the structures reported in this paper have been deposited with the Cambridge Crystallographic Data Centre as Supporting Information, CCDC numbers: 687241 (**1**), 687242 (**2**), and 687243 (**3**). Copies of the data can be obtained free of charge upon application to CCDC, 12 Union Road, Cambridge CB2 1EZ, United Kingdom (Fax: (44) 1223 336-033; e-mail: deposit@ccdc.cam.ac.uk).

Results and Discussion

Compounds **1**−**3** were synthesized under nearly identical conditions; however, the yield for the gadolinium compound, **1**, was significantly lower than that for the erbium and yttrium compounds, **2** and **3** (45% vs 75−80%), with the formation of Cu(*trans*-2-butenoate)₂ as a side product (see S1 in the Supporting Information). A similar reaction using Ho_2O_3 (Ho^{III} is 0.04 Å shorter than Gd^{III} for coordination number (CN) = 9) yielded the isostructural Cu_2Ho_2 compound in good yield, which was identified by elemental analysis and XRD. It appears that the synthetic reaction course is dependent on the size of the lanthanide ion. Shortening the ionic radii size[38] (CN = 9) from Gd^{III} to Er^{III}, Ho^{III}, and Y^{III} (0.05, 0.04, and 0.03 Å, respectively) changes from low to high yield reactions. Extension of this synthetic approach to lanthanides with ionic radii larger than Gd^{III} was unsuccessful. It appears that the lack of flexibility of monocarboxylates limits not only the formation of extended inorganic hybrids but also the range of different structures that may form in a given system. Steric reaction control is characteristic of lanthanide chemistry due to the contraction along the series, and many examples are reported in the literature.[39,40]

Crystal Structures. Compounds **1**−**3** are isostructural and crystallized in the centrosymmetric space group $P2_1/c$ with $Z = 4$. Crystal data and selected bond lengths and distances are listed in Tables 1 and 2, respectively.

The three compounds have similar structures, and Figures 1 and 2 show the dinuclear units and the noncentrosymmetric chain of **1** as a representative example of the group. The chains are built by two distinct units: two Cu^{II} ions bridged by four carboxylate bridges in the $\eta^1:\eta^1:\mu_2$ conformation, Figure 1a, and two Gd^{III} ions bridged by two carboxylate oxygen atoms in the $\eta^2:\eta^1:\mu_2$ conformation, Figure 1b. Each Cu^{II} atom of the Cu₂ dinuclear unit provides the basal plane for a square-pyramidal arrangement, the apical sites being provided by atoms O1I and O1F common to the Gd₂ coordination polyhedra. The Cu₂ unit resembles the structure of dinuclear Cu₂(L)₄(DMF)₂,[27] the main difference being the absence of an inversion symmetry center relating the copper

(29) Stoll, S. *Int. EPR Soc. Newsletter* **2003**, *13*, 24–26.
(30) Stoll, S.; Schweiger, A. *J. Magn. Reson.* **2006**, *178*, 42–55.
(31) *Matlab Matlab*; The Mathworks Inc.: Natick, MA.
(32) *SMART-NT*, V5.624; Siemens Analytical X-ray Instruments Inc.: Madison, WI, 2001.
(33) *SAINT-NT*, V6.22; Siemens Analytical X-ray Instruments Inc.: Madison, WI, 2001.
(34) Sheldrick, G. M. *SADABS*; Bruker AXS Inc.: Madison, WI, 2002.
(35) Sheldrick, G. M. *SHELXS 97*; *SHELXL 97*; University of Göttingen: Göttingen, Germany, 1997.
(36) *SHELXTL-NT*; Bruker AXS Inc.: Madison, WI, 2001.
(37) Allen, F. H. *Acta Crystallogr., Sect. B* **2002**, *B58*, 380–388.
(38) Shannon, R. D. *Acta Crystallogr., Sect. A* **1976**, *32*, 751–767.
(39) Schumann, H.; Meese-Marktscheffel, J. A.; Esser, L. *Chem. Rev.* **1995**, *95*, 865–986.
(40) Evans, W. J. *Inorg. Chem.* **2007**, *46*, 3435–3449.
(41) Baggio, R.; Garland, M. T.; Moreno, Y.; Peña, O.; Perec, M.; Spodine, E. *J. Chem. Soc., Dalton Trans.* **2000**, 2061–2066.

Table 1. Crystal and Structure Refinement Data for **1**, **2**, and **3**[a]

compound	**1**	**2**	**3**
empirical formula	$C_{40}H_{64}Cu_2Gd_2O_{27}$	$C_{40}H_{64}Cu_2Er_2O_{27}$	$C_{40}H_{64}Cu_2Y_2O_{27}$
fw	1418.49	1438.51	1281.81
cryst syst	monoclinic	monoclinic	monoclinic
a, Å	13.927(2)	13.872(1)	13.953(7)
b, Å	22.089(3)	22.068(2)	22.121(7)
c, Å	19.918(2)	19.839(1)	19.900(7)
β, deg.	107.19(1)	107.14(1)	107.16(3)
V, Å^3	5853.8(12)	5803.6(7)	5869(4)
Z	4	4	4
d_{calcd}, g cm^{-3}	1.61	1.65	1.45
cryst size	$0.38 \times 0.16 \times 0.14$	$0.34 \times 0.12 \times 0.12$	$0.26 \times 0.11 \times 0.10$
$F(000)$	2824	2856	2624
μ, mm^{-1}	3.03	3.66	2.75
θ range, deg.	1.41 to 28.04	1.84 to 28.10	2.80 to 27.99
data, R_{int}, parameters	13054, 0.052, 650	12922, 0.062, 650	12298, 0.071, 650
R1,[a] wR2[b] [$F^2 > 2\sigma(F^2)$]	0.042, 0.137	0.051, 0.122	0.058, 0.146
R1,[a] wR2[b] [all data]	0.050, 0.141	0.094, 0.136	0.136, 0.188
max and min peaks, e Å^{-3}	1.84, -1.05	1.33, -1.14	0.70, -0.40

[a] R1: $\sum||F_o| - F_c||/\sum|F_o|$. [b] wR2: $\{\sum[w(F_o^2 - F_c^2)^2]/\sum[w(F_o^2)^2]\}^{1/2}$.

Table 2. Selected Bond Distances [Å] for **1**, **2**, and **3**

	1	**2**	**3**
Ln1−O1W	2.362(4)	2.311(5)	2.322(6)
Ln1−O1G	2.363(4)	2.301(6)	2.318(6)
Ln1−O1J	2.402(4)	2.355(6)	2.355(6)
Ln1−O1H	2.418(5)	2.332(6)	2.369(6)
Ln1−O2I	2.421(5)	2.344(6)	2.382(6)
Ln1−O2W	2.432(4)	2.373(5)	2.390(5)
Ln1−O2J	2.453(4)	2.403(5)	2.421(6)
Ln1−O1I	2.624(4)	2.619(6)	2.646(6)
Ln1−O2H	2.723(4)	2.828(6)	2.837(7)
Ln2−O4W	2.350(4)	2.310(5)	2.319(6)
Ln2−O2H	2.381(4)	2.307(5)	2.303(6)
Ln2−O3W	2.402(4)	2.348(5)	2.367(5)
Ln2−O2F	2.415(4)	2.368(5)	2.361(5)
Ln2−O2E	2.419(4)	2.371(6)	2.393(6)
Ln2−O2G	2.439(4)	2.373(5)	2.376(5)
Ln2−O1E	2.464(4)	2.424(5)	2.438(6)
Ln2−O1F	2.641(4)	2.628(5)	2.640(5)
Ln2−O1G	2.633(4)	2.675(6)	2.674(6)
Ln1−Ln2	4.203(1)	4.214(1)	4.230(1)
Cu1−O1B	1.941(4)	1.938(6)	1.958(6)
Cu1−O1C	1.951(4)	1.950(6)	1.965(7)
Cu1−O1D	1.946(4)	1.959(6)	1.972(6)
Cu1−O1A	1.980(4)	1.978(6)	1.988(6)
Cu1−O1F#1	2.231(4)	2.223(5)	2.229(5)
Cu2−O2A	1.928(4)	1.933(6)	1.950(6)
Cu2−O2C	1.965(4)	1.970(6)	1.965(6)
Cu2−O2D	1.965(4)	1.958(6)	1.968(6)
Cu2−O2B	1.972(4)	1.990(6)	1.980(6)
Cu2−O1I	2.189(4)	2.183(6)	2.182(6)
Cu1−Cu2	2.645(1)	2.641(1)	2.654 (1)

[a] Symmetry code #1: $x - 1, y, z$.

ions, present in the latter. The four independent carboxylato bridges in the Cu$_2$ structure depart an average of 0.11 Å from a centrosymmetric disposition, as measured by the best fit of the dinuclear unit with its inverted image (XP in the SHELXTL package).[35] The four Cu−O−C−O−Cu loops are planar within 0.05 Å and are parallel or perpendicular to each other within a maximum deviation of ca. 3°. The Cu···Cu distance within the dinuclear unit is 2.645(1) Å compared with 2.613 Å in Cu$_2$(L)$_4$(DMF)$_2$,[27] and 2.616 Å in copper acetate monohydrate.[42]

In the Gd$_2$ unit (Figure 1b), the metal centers are bridged by two oxygen atoms from two tridentate carboxylates at a

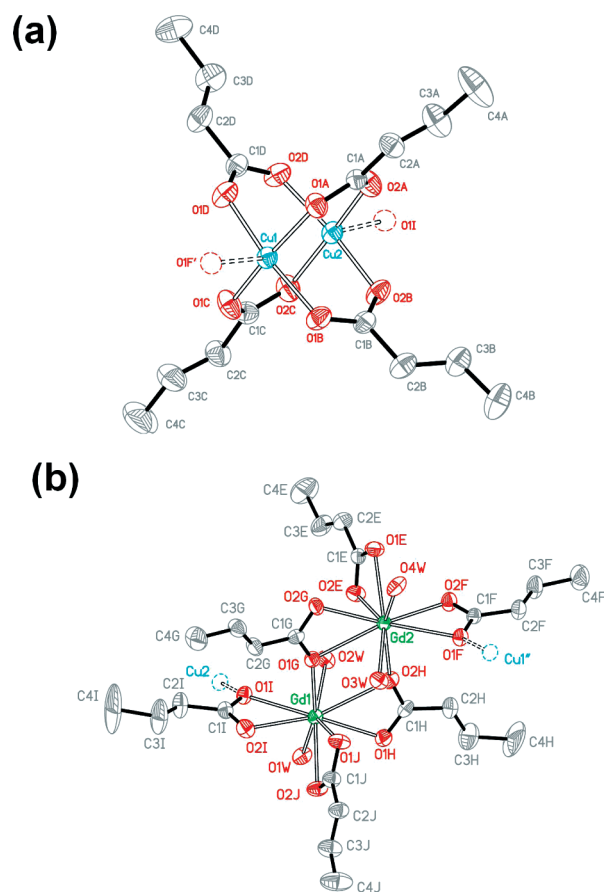(42) Van Niekerk, J. N.; Schoening, F. R. L. *Acta Crystallogr.* **1953**, *6*, 227–232.

Figure 1. Labeled molecular diagrams of the two building blocks in the **1** chain: (a) copper and (b) gadolinium. Displacement ellipsoids are drawn at a 40% probability level. Symmetry codes: ′ $x - 1, y, z$; ″ $x + 1, y, z$.

Gd···Gd distance of 4.203(1) Å. The coordination of each gadolinium (GdO$_9$) is completed by two chelating carboxylates and two aqua oxygens. Departure from a centrosymmetric arrangement is more important in this block than in the copper one, the mean deviation from the inverted image being 0.29 Å. Within a chain, Figure 2, alternate dinuclear units of the same type are related by a unit cell translation along a. All chains are symmetry-related, and the symmetry elements in the $P2_1/c$ space group are external. As a consequence, there are two slightly different Cu−Gd chemi-
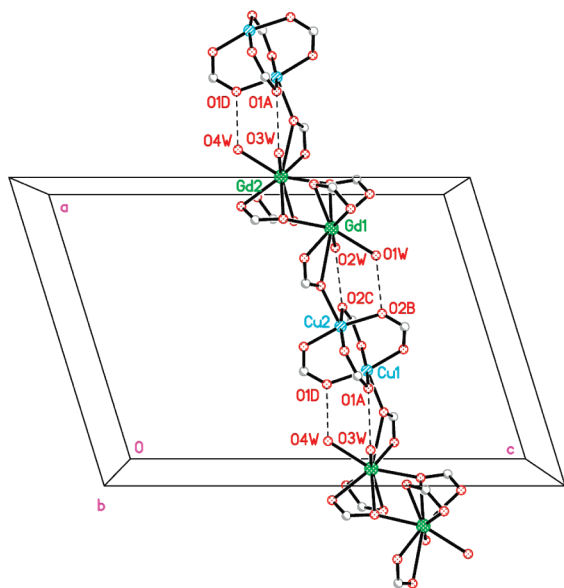
Figure 2. Schematic view of the structure along *a*, showing the way in which a chain of compound **1** builds up. Intrachain H bonds are shown with dashed lines. Atoms not involved in the chain formation are omitted, for clarity.

cal bridges with distances 4.496 and 4.517Å, respectively, between neighbor Cu and Gd ions. The Cu and Gd ions are bonded by a set of one covalent carboxylate oxygen and two H bonds.

Each chain is surrounded by six others, and the axis-to-axis separations between a chain and its neighboring ones cover the range 10−14 Å. The alkene groups protrude outward almost normal to the chain direction. Although hydrogen atoms of water molecules could not be found in the late difference Fourier maps, short $O_w \cdots O_{CO_2}$ and $O_w \cdots O_w$ distances less than 3.00 Å suggest involvement in H bonding. The intrachain H bonds connecting Cu_2 and Ln_2 units belong to aqua molecules.

EPR Spectroscopy. The EPR spectra of compounds **1**−**3** at 9.76 GHz and room temperature are displayed in Figure 3. The spectrum of Cu_2Y_2, **3**, is as expected for a Cu^{II} binuclear unit with large anisotropic spin−spin interaction. Only three (labeled A, B, and C in Figure 3) of the four peaks expected for the powder spectrum of an axially symmetric unit[43] are observed at this microwave frequency. The fourth peak at $g \sim 2.1$, labeled X in Figure 3, corresponds to a small amount of Cu^{II} mononuclear impurities (see below).

The EPR spectrum of compound **3** is described by the spin Hamiltonian:[43]

$$H_s = \mu_B B_0 \cdot \mathbf{g} \cdot S_1 + \mu_B B_0 \cdot \mathbf{g} \cdot S_2 - J_{Cu-Cu} S_1 \cdot S_2 + S_1 \cdot \mathbf{d} \cdot S_2 \quad (1)$$

where S_1 and S_2 are the 1/2 spins of the copper ions in a Cu_2 binuclear unit, **g** is the g matrix, assumed to be identical for the two coppers in the dinuclear units, J_{Cu-Cu} is the magnitude of the isotropic (Heisenberg) exchange coupling, and **d** is

(43) Weil, J. A.; Bolton, J. R.; Wertz, J. E. *Electron Paramagnetic Resonance. Elementary Theory and Practical Applications*; Wiley: New York, 1994.
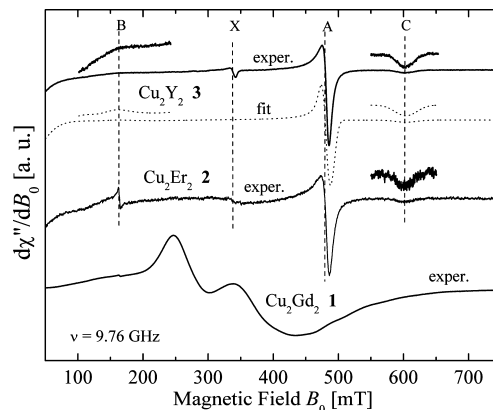
Figure 3. EPR spectra observed at 9.76 GHz and 300 K for **3**, **2**, and **1**. A spectrum simulated for **3** with the least-squares parameters given in the text is included. The insets amplify (×5) small peaks of the experimental and calculated spectra. Peaks A, B, and C belong to the Cu_2 dinuclear unit having approximate axial symmetry.[43] A fourth line of this set is missing at this microwave frequency. Peak X corresponds to monomeric Cu^{II} impurities.

the symmetrical traceless matrix considering the dipole−dipole coupling and anisotropic contributions to the exchange interaction, responsible for the energy splitting between singlet and triplet states and the zero-field splitting of the spin triplet, respectively. The diagonal matrix elements of **d** are related to the axial (D_0) and orthorhombic (E_0) zero-field-splitting parameters of the triplet state by[43]

$$D_0 = \tfrac{1}{2}[d_{zz} - \tfrac{1}{2}(d_{xx} + d_{yy})], \quad E_0 = \tfrac{1}{4}(d_{xx} - d_{yy}) \quad (2)$$

Assuming that the **g** and **d** matrices have the same principal axes, we calculated the spin Hamiltonian parameters using Easyspin,[29,30] fitting eqs 1 and 2 to the observed spectrum of **3** in Figure 3. By least-squares minimization, we obtained $g_{\parallel} = 2.350(3)$, $g_{\perp} = 2.054(3)$, $D_0 = -0.342(3)$ cm^{-1}, and $E_0 = 0.003(1)$ cm^{-1}, independent of J_{Cu-Cu}. We include the spectra simulated with Easyspin,[29,30] using the parameters given above. The g factors and the fine structure parameters are nearly identical to the values measured in the cases of copper acetate monohydrate ($D_0 = -0.34$ cm^{-1})[44,45] and Cu_2(*trans*-2-butenoate)$_4$(DMF)$_2$ ($D_0 = -0.335$ cm^{-1}).[27] The narrow signal at $B_0 \sim 0.33$ T is assigned to single copper impurities, and its amplitude is compatible with what is obtained for the same contribution from the magnetization data (see below).

The spectrum of Cu_2Er_2, **2**, is very similar to that of Cu_2Y_2, **3**, as observed previously with other CuLn compounds with fast-relaxing open-shell lanthanides.[46] Very low temperature measurements would be needed to slow down the relaxation of the Er^{III} ions and, simultaneously, to freeze the Cu dimeric units in their $S = 0$ ground states. In that case, one may expect to obtain information about the Er^{III} ions and about the Er_2 dinuclear unit.

As a consequence of the coupling between Cu and Gd dinuclear units and the long relaxation times of the Gd ions,

(44) Bleaney, B.; Bowers, K. D. *Proc. R. Soc. London* **1952**, *A214*, 451−465.
(45) Figgis, B. N.; Martin, R. L. *J. Chem. Soc.* **1956**, *1956*, 3837−3846.
(46) Rizzi, A.; Calvo, R.; Baggio, R.; Garland, M.; Peña, O.; Perec, M. *Inorg. Chem.* **2002**, *41*, 5609−5614.
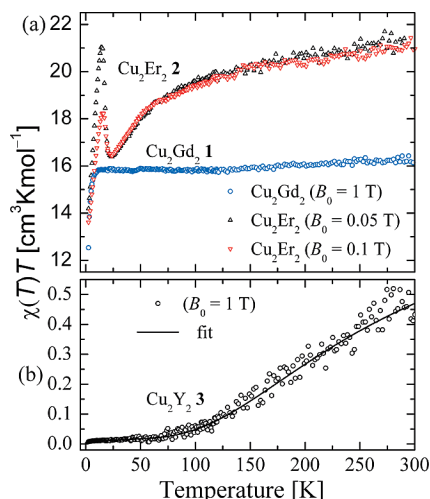
Figure 4. Product $\chi(T) \cdot T$ as a function of T for (a) Cu$_2$Er$_2$, **2**, and Cu$_2$Gd$_2$, **1**, and (b) for Cu$_2$Y$_2$, **3**. The magnetic field at which the data were obtained is indicated. The height of the peak at 15 K for Cu$_2$Er$_2$ changes with the magnetic field. The solid line with the data for **3** is obtained using the parameters obtained from the fitting of the magnetization data.

the spectrum of **1** is not the superposition of the spectra of Cu and Gd dinuclear units, but it shows a complex profile, as expected for a chain containing two 1/2 spins and two 7/2 spins. Even assuming that the spin Hamiltonian parameters for the Cu$_2$ dinuclear unit are equal to those obtained for **3**, a simulation of the EPR powder spectrum of **1** should include several zero-field-splitting parameters for the $S = 7/2$ Gd ions, plus the exchange and dipolar couplings between Gd ions and between Cu and Gd ions, and this was not attempted.

Magnetic Results. The magnetic susceptibilities, $\chi(T)$, of Cu$_2$Gd$_2$ (**1**), and Cu$_2$Er$_2$ (**2**), and Cu$_2$Y$_2$ (**3**) are plotted as $\chi(T) \cdot T$ in Figure 4a and b, respectively. The molar magnetizations, M_m, of these compounds were measured for several values of the applied magnetic fields, B_0, between 0.05 and 9 T for temperatures T between ~2 and 300 K. The measured magnetic moment M_m/N_{Av} in Bohr magnetons as a function of T per Cu$_2$Ln$_2$ block are displayed in Figures 5a, 6a, and 7. Figures 5b and 6b display the isothermal magnetization curves, M_m/N_{Av}, for **1** and **2** at various values of T, as a function of B_0. The diamagnetic and temperature-independent paramagnetic (TIP) contributions have not been subtracted in Figures 5−7 but will be considered in the later analysis. They are not relevant (<0.7%) for **1** and **2**, where the larger contributions of the lanthanide ions dominate, but are relevant for **3**, where the negative diamagnetic contribution to the magnetization predominates in the low-temperature range.

For **1**, $\chi(T)$ is within experimental accuracy, field-independent at low fields, and the data shown in Figure 4a were obtained at 1 T. At high T, $\chi(T) \cdot T$ is ~ 16.2 cm^3 K/mol and temperature-independent, as expected for a Cu$_2$ dinuclear unit (~0.5 cm^3 K/mol), plus two Gd^{III} free ions with $S = 7/2$ and $g = 1.99$ (~15.6 cm^3 K/mol).[15] Below 10 K, when the contribution of the strongly antiferromagnetically coupled Cu^{II} dinuclear unit is negligible, the susceptibility decreases with decreasing temperature, indicating predominant antiferromagnetic arrangement of the Gd ions at low temperatures. At the maximum field, B_0, and the lowest temperature,
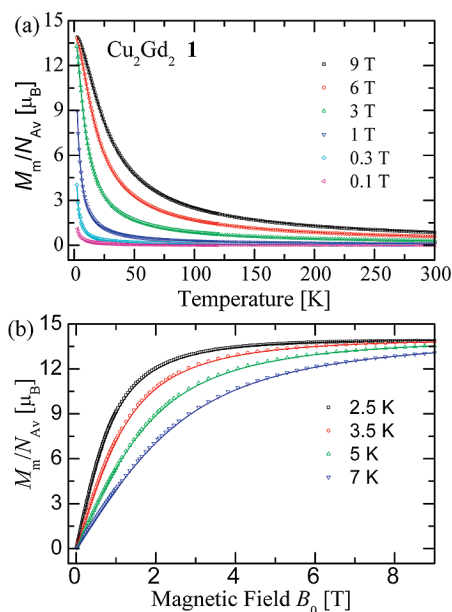
Figure 5. (a) Molecular magnetic moment of **1** for several values of the applied magnetic field measured as a function of the temperature. (b) Molecular magnetic moment of **1** as a function of B_0 at $T = 2.5, 3.5, 5,$ and 7 K. The symbols are experimental values. The solid lines are calculated with the parameters obtained from a least-squares fit of eqs 7−11 to the data in parts a and b and given in the text.
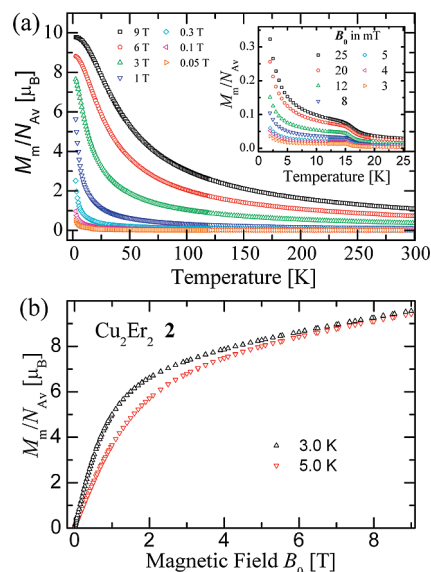

Figure 6. (a) Observed molecular magnetic moment of **2** as a function of the temperature measured for several values of the applied magnetic field. The inset displays the magnetic moment for small applied magnetic fields B_0 as a function of T around 15 K, where a peak in $\chi(T) \cdot T$ is observed. (b) Molecular magnetic moment of **1** as a function of B_0 for several values of the applied magnetic field, as a function of T.

T, the magnetization, M_m/N_{Av}, for **1** (Figure 5b) approaches 14 μ_B, equal to the saturation value expected for two free Gd^{III} ions ($S = 7/2$ and $g \sim 1.99$). At these temperatures and fields, and according to the data for **3** (see Figure 7), the contribution of the Cu$_2$ unit is negligible.

As shown in Figure 4a for **2**, $\chi(T) \cdot T$ at $B_0 = 0.05$ and at 0.1 T displays a peak at $T \sim 15$ K. Even at these low fields, the value at this peak depends on the magnetic field of the measurement $\chi(T) \cdot T \sim 21.3$ cm^3 K mol^{-1} at 300 K (Figure 4a), still increasing with increasing temperature. This value
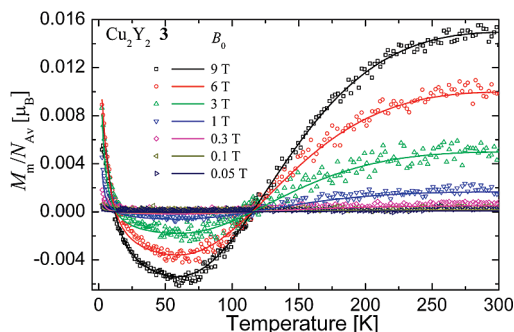
Figure 7. Temperature variation of the molecular magnetic moment of **3** for several fixed values of the magnetic field. Symbols are experimental results. The solid lines are obtained from a least-squares fit of eqs 3−6 to the data. The parameters obtained are given in the text.

is close to the ∼24 cm³ K mol⁻¹ expected for two Er^{III} ions plus two Cu^{II} ions at temperatures where all crystal field levels of the ground multiplet having $J = 15/2$ are populated. Upon lowering the temperature, $\chi(T)\cdot T$ decreases to 16 cm³ K mol⁻¹ at 25 K, increases again to a peak value of 21 cm³ K mol⁻¹ at 15 K, and falls steeply to 14 cm³ K mol⁻¹ at 2 K. As occurs for the Gd compound, this decrease indicates a predominant antiferromagnetic arrangement of the Er ions at low temperatures. The minimum of $\chi(T)\cdot T$ at 25 K and the peak value at 15 K observed for **2** reflect the more complicated behavior of the open-shell lanthanide.[18]

The saturation value $M_m/N_{Av} \sim 9.5$ μ_B observed at high fields for the magnetic moment of a molecule of **2** should be compared with the value $M_m/N_{Av} \sim 18$ μ_B expected for the $J = 15/2$ of the ground multiplet of Er^{III} and the reduced g value $g_J = 6/5$ of the multiplet.[15,47] The smaller experimental result is a consequence of the reduction produced by the crystal field splitting. Also, the smaller value of $\chi(T)\cdot T$ with a temperature for **2** around 300 K is attributed to the depopulation of the higher crystal field levels of Er^{III}. The peak at 15 K is more difficult to rationalize; to clarify its origin, we also measured the magnetization of **2** with small applied fields as a function of a temperature of around 15 K (see inset of Figure 6a) at several small values of B_0. At low T, the strongly coupled Cu₂ unit is in its ground singlet state, and the Er₂ unit is magnetically isolated. Considering the weak Ln−Ln interactions and the 1-D spin chain structure of **2**, one can hardly explain a magnetic transition peak in $\chi(T)\cdot T$ at 15 K. It seems more appropriate to assume that the interactions between Er ions in the dinuclear units are antiferromagnetic, and so the ground state of the Er₂ unit is a singlet, not a magnetic state, followed by an excited triplet. This explains the small value of $\chi(T)\cdot T$ at low T, rapidly increasing up to 15 K, when excited states of the Er₂ dinuclear units become populated. However, the existence of a coupling (either ferromagnetic or antiferromagnetic) between Cu and Er neighbors in the chain and the magnetic moment of the Cu₂ units that increases with T produce the peak and the reduction of $\chi(T)\cdot T$ between 15 and 25 K, as the result of the two competing contributions. At higher temperatures, the behavior is similar to that of **1**, except that

there is an additional increase in the population of the excited crystal field states with increasing T. This qualitative explanation predicts a reduction of the peak at 15 K due to a field-induced broadening.

The magnetic susceptibility of **3**, Figure 4b, is very small, as expected for a strongly antiferromagnetic dinuclear unit of 1/2 spin. The magnetization curves of **3**, Figure 7, are typical of a copper dinuclear compound with a large antiferromagnetic coupling.[15] Below 50 K, the curve increases with decreasing temperature as a consequence of the presence of paramagnetic mononuclear copper(II) in the sample (see below). In the following section, we analyze with greater detail the behavior of the magnetization of **1** and **3** (Figures 5 and 7) and obtain the exchange interaction parameters.

Modeling the Magnetic Behavior. The local coordination environments of the copper dinuclear units of the isostructural compounds **1**−**3** are very similar to each other, allowing comparative studies of the magnetic roles of individual lanthanides in the same host. Since yttrium(III) is nonmagnetic, the molar susceptibility of Cu₂Y₂ (**3**) as a function of the temperature follows the equation of Bleaney and Bowers.[15,44,47] The molecular magnetic moment, M_{Cu_2}/N_{Av}, of Cu₂ dinuclear units of **3** at field B_0 and temperature T, displayed in Figure 7, can be written as

$$M_{Cu}(B_0, T)/N_{Av} = 2g_{Cu}\mu_B \exp(J_{Cu-Cu}/k_BT) \sinh(g_{Cu}\mu_B B_0/k_BT)/Z \quad (3)$$

where J_{Cu-Cu} is defined in eq 1 and the partition function Z is

$$Z = 1 + \exp(J_{Cu-Cu}/k_BT)[1 + 2\cosh(g_{Cu}\mu_B B_0/k_BT)] \quad (4)$$

In eqs 3 and 4, g_{Cu} is the angular average of the anisotropic g factor of the copper ions. Considering the presence of a small fraction, ρ, of mononuclear paramagnetic copper centers, the observed reduced magnetization of **3** can be written as[15]

$$M_{Cu_2Y_2}(B_0, T) = (1 - \rho)M_{Cu_2} + \rho M_{param} + \chi(TI) B_0 \quad (5)$$

The paramagnetic contribution[15] to eq 5 is expressed by

$$M_{param}(B_0, T)/N_{Av} = g_{Cu}\mu_B \tanh(g\mu_B B_0/2k_BT) \quad (6)$$

The last term of eq 5 is important at low T when M_{Cu2} of eq 3 is very small for an antiferromagnetically coupled unit. This term accounts for the diamagnetic and temperature-independent contributions. The data in Figure 7 were analyzed using eqs 3−6, and since diamagnetic and temperature-independent contributions are dominant compared with other contributions to eq 5, we consider them as a single adjustable parameter, $\chi(TI)$, added to this equation.

A least-squares fit of eq 5 to the data in Figure 7 allows for obtaining

$$g_{Cu} = 2.11 \pm 0.01, \; J_{Cu-Cu} = (-338 \pm 3) \text{ cm}^{-1}, \; \rho = 0.72\%, \; \chi(TI) = -4.5 \times 10^{-4} \text{ cm}^3/\text{mol}$$

The solid lines in Figures 3 and 7, calculated with these values, reproduce the experimental results at the different magnetic fields within the experimental accuracy.

(47) Abragam, A.; Bleaney, B. *Electron Paramagnetic Resonance of Transition Ions*; Oxford University Press: Oxford, 1970.

The information about the Cu_2 units in compound **3** is helpful to model the properties of **1** and **2**. If the Cu_2 and Ln_2 units were well isolated with no interaction, their magnetic properties should be the sum of those expected for these units, and since the contribution of strongly antiferromagnetically coupled Cu_2 units is very small, the magnetic response at very low temperatures would be dominated by the Ln_2 contribution. However, if the exchange interactions between Cu and Ln in neighboring dinuclear units are not negligible, the bulk magnetic behavior of **1** and **2** may be strongly dependent on the coupling within the Cu_2 unit, even if its individual contribution is negligible compared with that of the Gd ions.

Considering the structure of the three isostructural complexes, our results here reported for **3**, and existing information about exchange interactions in dinuclear Gd_2 compounds[26,48] and in compounds containing Cu and Gd ions,[49] it is to be expected that $(1/2)^2|J_{Cu-Cu}| \gg (7/2)^2|J_{Gd-Gd}|$, $(1/2)^2|J_{Cu-Cu}| \gg (7/4)|J_{Cu-Gd}|$, and $(7/4)|J_{Cu-Gd}| \gg (7/2)^2|J_{Gd-Gd}|$ (the numerical factors consider the spins 1/2 and 7/2 of Cu^{II} and Gd^{III}, respectively).

The approximation of noninteracting Cu_2 and Gd_2 dinuclear units did not explain the magnetic results. Thus, the method of Bonner and Fisher[50] would be indicated for treating numerically the magnetic properties of spin chains. If the interaction between Cu and Gd neighbors in the spin chains of **1** is more important than the interaction between neighboring Gd ions,[51] the spin chain displayed in Figure 2 may be interpreted as breaking up into weakly interacting tetranuclear blocks Gd−Cu−Cu−Gd. Thus, we neglected interchain interactions and the small differences between the two Cu−Ln bonds assuming that J_{Cu-Ln}'s have equal magnitudes. With this assumption and within the approach of Bonner and Fisher,[50] one could model the magnetic behavior of **1** considering chains of weakly interacting tetranuclear Gd−Cu−Cu−Gd blocks. The spin Hamiltonian for such a block is

$$H_0 = -J_{Cu-Cu}S_{Cu_1} \cdot S_{Cu_2} - J_{Cu-Gd}(S_{Cu_2} \cdot S_{Gd_1} + S_{Gd_2} \cdot S_{Cu_1}) + g_{Cu}\mu_B(S_{Cu_1} + S_{Cu_2}) \cdot B + g_{Gd}\mu_B(S_{Gd_1} + S_{Gd_2}) \cdot B \quad (7)$$

Neighboring blocks in a chain are coupled by the Gd−Gd exchange interaction, J_{Gd-Gd}, giving rise to the spin chain:

$$H' = -J_{Gd-Gd}S_{Gd_1} \cdot S_{Gd_2} \quad (8)$$

Calculation of the magnetic properties should involve n tetranuclear blocks, with the quality of the result increasing with n.[50] So, we carried out full least-squares fittings with $n = 1$; estimations with $n = 2$ showed that the $n = 1$ approximation is satisfactory, as a consequence of the large difference between the magnitudes of the couplings.

To model magnetization results at large magnetic fields, full-matrix diagonalization is required instead of a "vectorial"

model valid for calculating magnetic susceptibilities.[15,52] The 256 energy levels of the tetranuclear block containing two 1/2 spins and two 7/2 spins were obtained from the Hamiltonian of eqs 7 and 8, expressed as product functions $|m_{Gd1}\, m_{Cu_1}\, m_{Cu_2}\, m_{Gd2}>$ of the spin quantum numbers m_i, as a function of the parameters J_{Cu-Cu}, J_{Cu-Gd}, J_{Gd-Gd}, g_{Cu}, and g_{Gd}. The magnetic moment operator for the block is

$$M_z = \frac{\partial H_0}{\partial B_0} = -\mu_B[g_{Cu}(m_{Cu_1} + m_{Cu_2}) + g_{Gd}(m_{Gd_1} + m_{Gd_2})]$$
$$(9)$$

where g_{Gd} is essentially isotropic and g_{Cu} is taken as the angular average of the copper g matrix, as for **3**. The magnetic moment $M(B_0,T)$ of one tetranuclear block with a magnetic field along z is

$$M(B_0,T) = <M_z> = \frac{1}{Z}Tr\left[M_z \exp\left(-\frac{H_0}{k_BT}\right)\right] \quad (10)$$

with the partition function

$$Z = Tr\left[\exp\left(-\frac{H_0}{k_BT}\right)\right] \quad (11)$$

Thermal averages of $<M_z>$ in eq 10 may be obtained using eqs 7 and 9. Considering eqs 7 and 8, we evaluated the parameters of a single tetranuclear block ($n = 1$) by minimizing the mean-square deviation between the experimental values of the magnetization in Figure 5a and b and the values calculated using eqs 10 and 11. g_{Gd}, J_{Cu-Gd}, and J_{Gd-Gd} were taken as variable parameters, and g_{Cu} and J_{Cu-Cu} were as determined for compound **3**. We obtained

$$g_{Gd} = 1.991, J_{Cu-Gd} = 13.0 \text{ cm}^{-1}, \text{ and } J_{Gd-Gd} = 0.25 \text{ cm}^{-1}$$
$$(12)$$

where J_{Cu-Gd} and J_{Gd-Gd} are ferromagnetic interactions.

Conclusions

We have prepared and characterized three new self-catenated monocarboxylate compounds $[Cu_2Ln_2L_{10} \cdot (H_2O)_4 \cdot 3H_2O]_n$ (Ln = Gd (**1**), Er (**2**), Y (**3**)) showing a linear alternation of Cu_2 and Ln_2 dinuclear units, bridged by carboxylate linkages.

The magnetic susceptibilities of the three compounds at low temperatures indicate bulk antiferromagnetic behavior. The strong antiferromagnetic behavior of **3** is similar to that obtained for other 4-fold bridged carboxylate Cu_2 units. Considering the similarities of the three structures, the results for the Cu_2 unit in **3** are used to interpret the data in compounds **1** and **2**. We modeled the magnetization data for compound **1**, assuming chains of tetranuclear blocks −Gd−Cu−Cu−Gd−, weakly exchange-coupled through the Gd−Gd bonds in the Gd_2 units, predicting susceptibility and magnetization curves in excellent agreement with the data. The exchange couplings between Cu−Gd neighbors at ∼ 4.5 Å are transmitted through a set of one covalent $\eta^2:\eta^1:\mu_2$

(48) Roy, L. E.; Hughbanks, T. *J. Am. Chem. Soc.* **2006**, *128*, 568−575.

(49) Costes, J.-P.; Dahan, F.; Dupuis, A. *Inorg. Chem.* **2000**, *39*, 165−168.

(50) Bonner, J. C.; Fisher, M. E. *Phys. Rev.* **1964**, *135A*, 640−657.

(51) Costes, J.-P.; Auchel, M.; Dahan, F.; Peyrou, V. S. S.; Wernsdorfer, W. *Inorg. Chem.* **2006**, *45*, 1924−1934.

(52) Novitchi, G.; Shova, S.; Caneschi, A.; Costes, J. P.; Gdaniec, M.; Stanica, N. *Dalton Trans.* **2004**, 1194−1200.

carboxylate oxygen and two H bonds, with the coupling values being consistent with those obtained by other authors.[16−18,26] The bulk antiferromagnetic behavior of compound **1** is attributed to the combined effect of the strong antiferromagnetic behavior within the Cu_2 unit, transmitted to the Gd ions by the coupling J_{Cu-Gd}. The detailed fit of the tetranuclear block model indicates that this coupling is ferromagnetic, as it is the Gd−Gd exchange coupling.

The complexity of the Er^{III} crystal field splitting does not allow a detailed calculation of the exchange couplings, as for compound **1**. We interpret the susceptibility peak as resulting from the competition of (*i*) an antiferromagnetic coupling within the Er_2 unit generating a nonmagnetic ground singlet state and (*ii*) a reduction in the susceptibility above 15 K when the two Er spins next to a Cu_2 unit tend to take opposite orientations. In the EPR spectrum of **2**, the contribution of the Er^{III} ions is averaged out due to their fast spin−lattice relaxation, showing only the Cu_2 signals. This does not occur for compound **1**, where Gd ions relax slowly, and the Cu−Gd interactions produce a distinctive collective EPR spectrum of the chains.

Supporting Information Available: X-ray crystallographic files in CIF format for compounds **1**, **2**, and **3** and EA and XRD characterization of the side product in the synthesis of compound **1**. This material is available free of charge via the Internet at http://pubs.acs.org.

IC8014089